Electronic Supplementary Material (ESI) for ChemComm.

Supplementary Information

Fabrication of stable lithium metal anodes using HF scavenging Films

Sungjin Cho, [‡a] Hye Bin Son, [‡a] Sangyeop Lee[b] and Soojin Park[*a,b]

Methods

Materials. Linear Polyethyleneimine (PEI) with an average molecular weight of 250,000 g/mol was purchased from Sigma-Aldrich. 3-(triethoxysilyl)propyl isocyanate (ICPTES) was purchased from Alfa-Aeser (95%). Dibutyltin dilaurate (DBTDL) (Sigma-Aldrich, 95%) was used as a catalyst in the urethane reaction. Pure ethyl alcohol (anhydrous >99.5%) was used as a solvent during the reaction. Then, 1.3 M $LiPF_6$ into ethylene carbonate/diethyl carbonate (EC/DEC = 3/7, v/v) with 10 wt% fluoroethylene carbonate (FEC) additive was purchased from Soulbrain. $LiMn_2O_4$ (LMO, Umicore) and $LiNi_{0.8}Co_{0.1}Mn_{0.1}O_2$ (NCM811, L&F) were used as the cathode. The commercial separator (Celgard 2400) was purchased from Celgard, and Li metal (thickness 100 μm) was purchased from Hosen Corporation. The conducting agent, carbon black Super P, was obtained from the Imerys. Poly(vinylidene fluoride) (PVDF, KF1100, Mn = 168.8 kDa, polydispersity index = 2.94, KUREHA Chem. Ind.) was used as the polymeric binder to make the cathode electrode. The solid electrolyte, Li_6PS_5Cl (LPSCl, Argyrodite) was purchased from the CIS.

Preparation of PETES solution and the films. PEI was dissolved in ethanol to yield 0.7 wt.% solutions and stirred at 25 °C for 1 h. 1.0 mmol of ICPTES and 0.080 mmol of DBTDL were added to the as-prepared PEI solution to synthesize the PETES. Subsequently, the solution was continuously stirred for 24 h at room temperature. The PETES solution was spin-coated onto the Cu and Ni foil surface at 2000 rpm for 60s to prepare the PETES film.

Preparation of Li metal anodes. Cu//Li or Ni//Li half cells were fabricated to prepare electrodeposited Li metal anodes. 8 mAh cm^{-2} Li was electrochemically plated on the current collector at a current density of 0.2 mA cm^{-2} for 40 h. The Cu//Li or Ni//Li cells were disassembled, and subsequently-electrodeposited Li was washed with dimethyl carbonate to clean the surface of the electrodes. The eLi-PETES anode was fabricated using PETES-Cu and PETES-Ni in the same method mentioned above.

Material characterization. The PETES formation was examined by FT-IR analysis using Agilent Cary 600 FTIR spectrometer. The surface topography of thin films was imaged using AFM (Park Systems, XE-70) in the non-contact mode. A stylus profilometer (Bruker DektakXT) was employed to measure the coating layer thickness. The AFM and DEKTAK samples were prepared on the cleaned silicon wafers by the spin-coating process, then kept in a vacuum oven to prevent contamination before examinations. XPS analysis was performed on an ESCALAB 2500 instrument (Thermo Fisher Scientific). SEM images of all the samples were obtained with a JSM-7800F Prime Field Emission Scanning Electron Microscopy (JEOL) at a 5 kV acceleration voltage. ICP-OES measurements were performed with the 700-ES (Varian).

Electrochemical measurements. All electrochemical investigations in liquid electrolytes were performed using CR2032-type coin cells and Celgard 2400 as the separator. All the cells were rested for 16 h before testing to allow the electrodes to be fully immersed in the electrolytes and were built in an argon-filled

glove box. Carbonate-based electrolytes containing 1.3 M $LiPF_6$ in EC/DEC (3/7, v/v) with 10% FEC additive were used. All experiments in the liquid electrolytes were performed at a constant temperature of 25 °C. Cu//Li half cells were coupled with Li metal as the counter electrode and the bare Cu current collector (20 μm, Hoshen) or PETES-Cu as the working electrodes. To measure the CEs during the Li deposition/stripping, the activation cycle was conducted at a current density of 0.5 mA cm^{-2} with an areal capacity of 4 mAh cm^{-2} for 1 cycle, followed by 1C at a current density of 1 mA cm^{-2} based on an area of Li metal. NCM 811 (areal density of 3.5 mAh cm^{-2}) and LMO (areal density of 1.3 mAh cm^{-2}) were used as the cathodes, and either eLi-Cu or eLi-PETES was used as the counter electrode. NCM811 full cells were assessed at a potential window between 2.5 and 4.2V using a Wonatech battery cycler (WBCS3000). The pre-cycle was conducted at 0.1 C for 1 cycle, followed by charging/discharging at 0.5 C. When the voltage of all the cells reached 4.2 V, a constant voltage charging process was used until the charge current decayed to 0.05 C. The 1 C rate corresponds to 3.5 mA cm^{-2} in all the full cells. LMO full cells were assessed at the potential window between 3.0 and 4.3V using a Wonatech battery cycler (WBCS3000). The pre-cycle was conducted at 0.1 C for 1 cycle, followed by a charging/discharging at the 1C rate. When the voltage of all the cells reached 4.3 V, a constant voltage charging process was used until the charge current decayed to 0.05 C. EIS was obtained using a multichannel potentiostat (VSP-300; Bio-Logic) with a frequency range of 10^{-3}–10^{6} Hz and an amplitude of 10 mV.

All-solid-state batteries. Coin-type ASSBs were fabricated using 8 mm diameter Li metal (thickness 100 μm, Hosen Corporation) as the counter electrode and 12 mm diameter eLi-Ni or eLi-PETES as the working electrodes to test the eLi-PETES or eLi-Ni // LPSCl // Li asymmetric cells. All electrochemical investigations in ASSBs were performed using CR2032-type coin cells. 120 mg of SE was placed in a mold (polyether ether ketone, 12 mm diameter) and cold-pressed at 100 MPa for 1 min to make SSE pellets for the coin-type ASSBs. To fabricate coin-type ASSBs, SSE pellets were placed between the working electrode and the counter electrode, and unlike the liquid electrolyte cell, a separator and liquid electrolyte were not used. Due to the thickness of the 2032 spacer and the SSE pellet, the spring pressure inside the coin cell was maximized to realize an internal pressure of about 5MPa. The ASSBs were rested at 70 °C for 10 h and at 25 °C for 10h. ASSACs were charged and discharged at a 1 C rate with a current density of 0.2 mA cm^{-2} based on an area of Li metal at 25°C to measure the overpotential during the Li deposition/stripping. About 120 mg of SE was pressed into pellet shape with a diameter of 12 mm under 495 Mpa for ionic conductivity measurement. Two In foils (thickness 100 μm) with a diameter of 12 mm were attached to the pellets under 125 Mpa as current collectors. EIS was obtained using a multichannel potentiostat (VSP-300; Bio-Logic) with a frequency range of 10^{-1}–10^{6} Hz and an amplitude of 10 mV. The test temperature was 25℃.

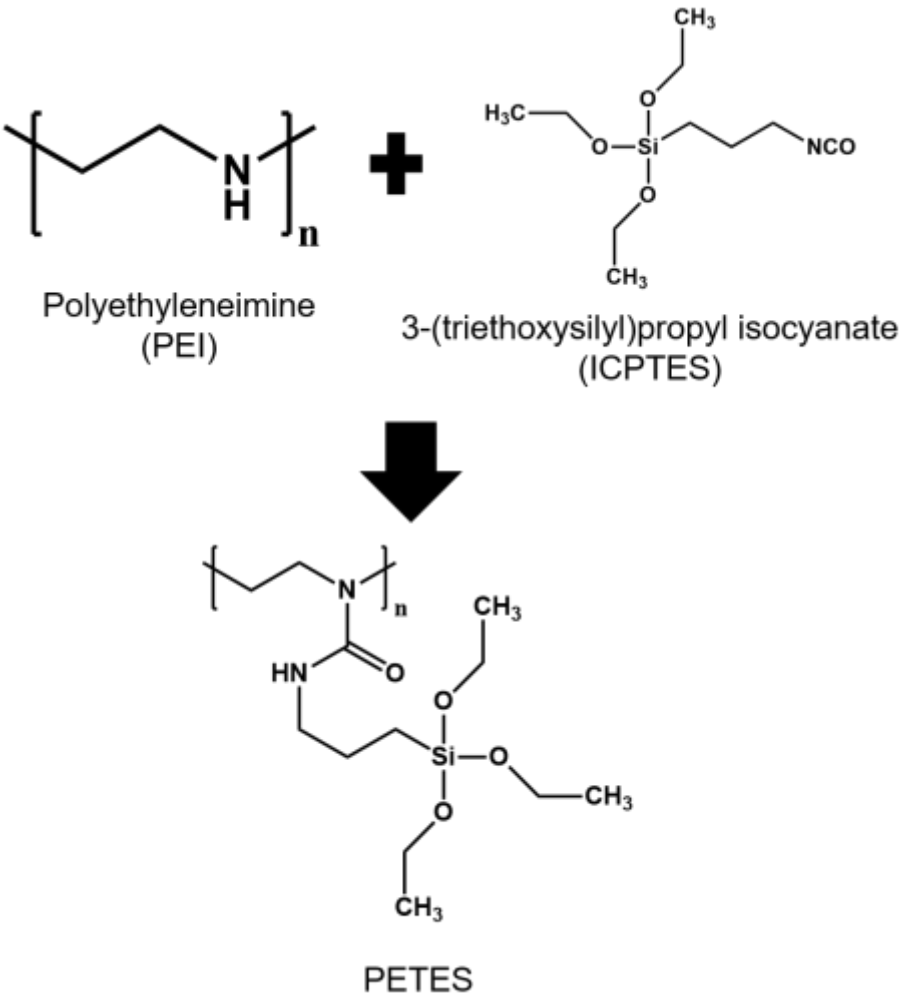

Fig. S1. The reaction mechanism of PETES formation.

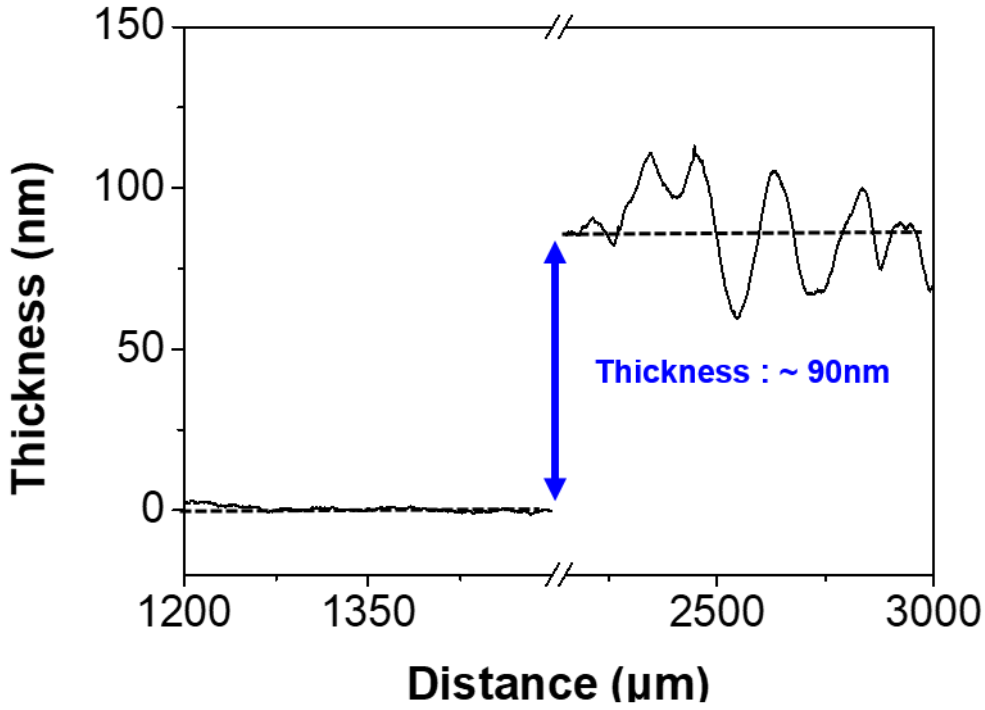

Fig. S2. The DEKTAK profile to measure the thickness of the PETES film.

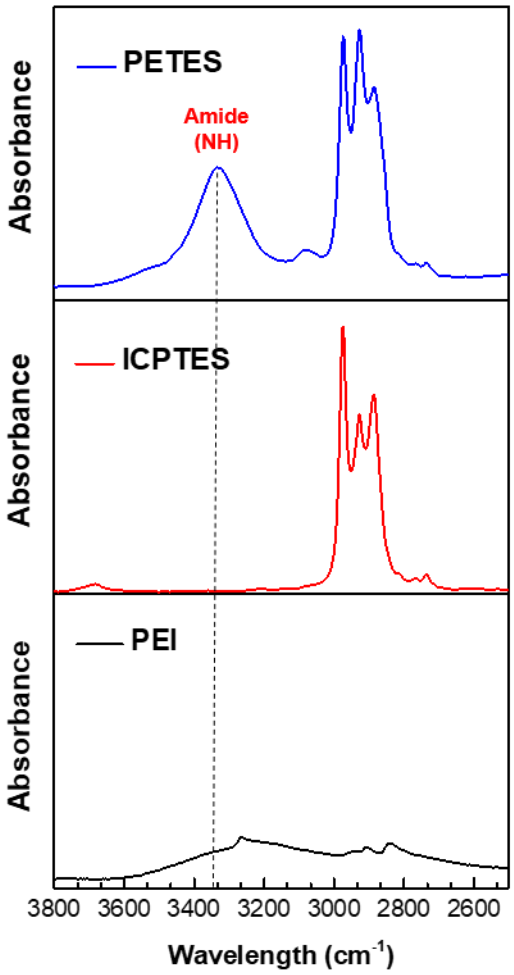

Fig. S3. FT-IR spectra of PETES, ICPTES, and PEI solutions in the high wavelength range.

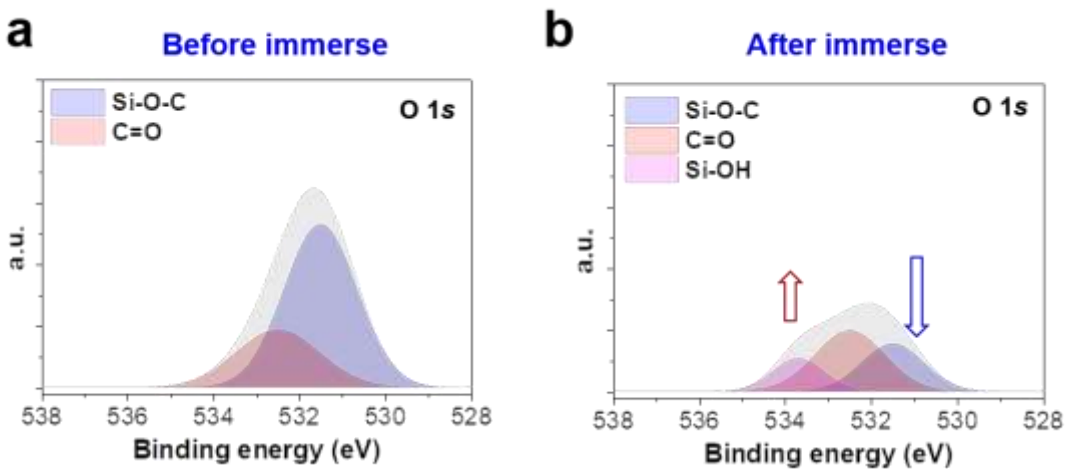

Fig. S4. O 1s XPS spectra of **a** the fully dried PETES-Cu electrode surface and **b** the PETES-Cu electrode surface after immersion in the fresh electrolyte. For the experiment, the PETES electrode was immersed in 1.3M $LiPF_6$-EC/DEC (3/7, v/v) with 10 wt% FEC electrolyte, and the change in the chemical composition of the polymer was checked after 10h. As a result, it was confirmed that the Si-O-C portion of the PETES-Cu electrode was greatly reduced due to a small HF amount, and Si-OH groups were formed by reacting with a small moisture amount.

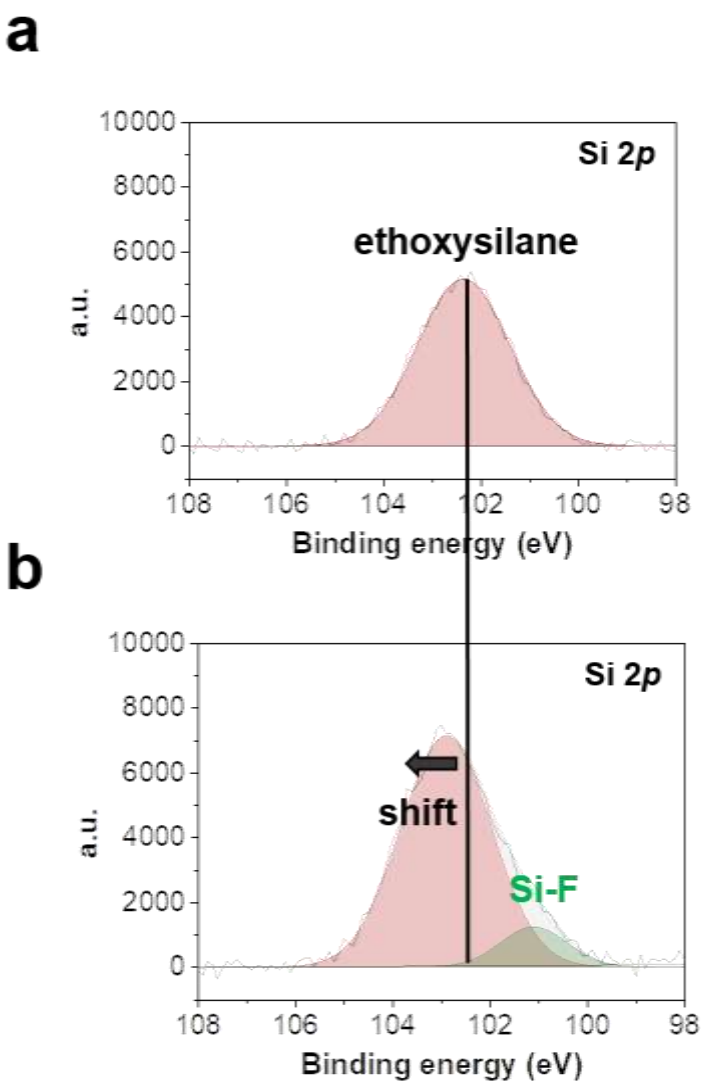

Fig. S5. Si 2p XPS spectra of fully dried PETES-Cu electrode surface after dropping **a** bare electrolytes and **b** water-containing electrolytes. For the experiment, water-contaminated electrolytes were prepared by dropping 2000 ppm of water into 400 µl of 1.3M $LiPF_6$-EC/DEC (3/7, v/v) with 10 wt% FEC. After that, 300 µl of the solution was dropped on bare Cu and PETES-Cu with an area of 3×3 cm^2 and dried for 10 minutes. This coating process was repeated three times.

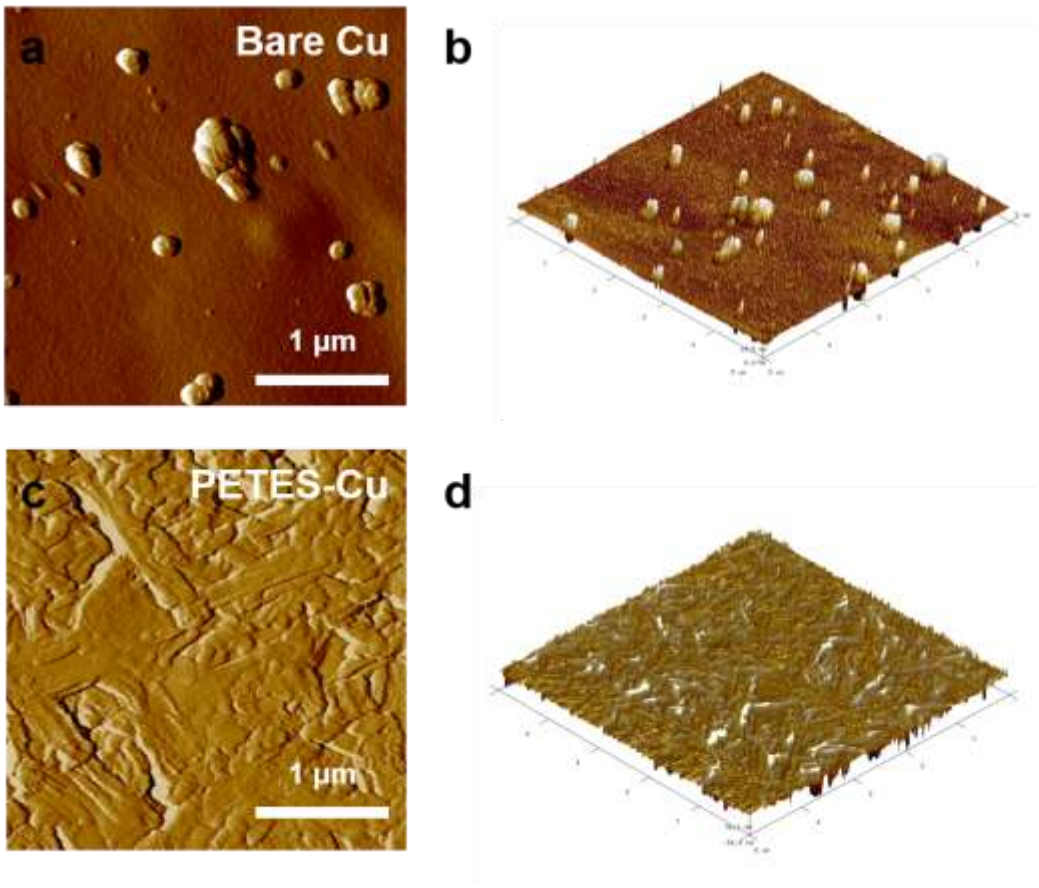

Fig. S6. AFM images of the working electrode after the initial cycle with a capacity of 4 mAh cm^{-2} at a current density of 0.5 mA cm^{-2}. **a** Top and **b** three-dimensional (3D) AFM images of the bare Cu electrode. **c** Top and **d** 3D AFM images of the PETES-Cu electrode.

a

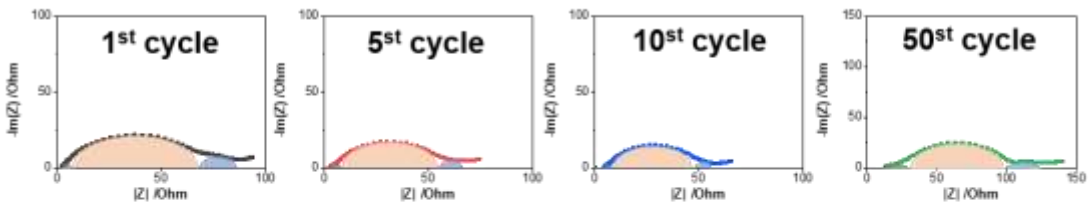

After lithiation (1mAh cm^{-2})	R_b (Ohm)	R_{SEI} (Ohm)	R_{CT} (Cu@Li + Li) (Ohm)
1st Cycle	2.37	5.63	78
5th Cycle	2.73	5.27	58
10th Cycle	4.58	4.42	50
50th Cycle	11	20	93

b

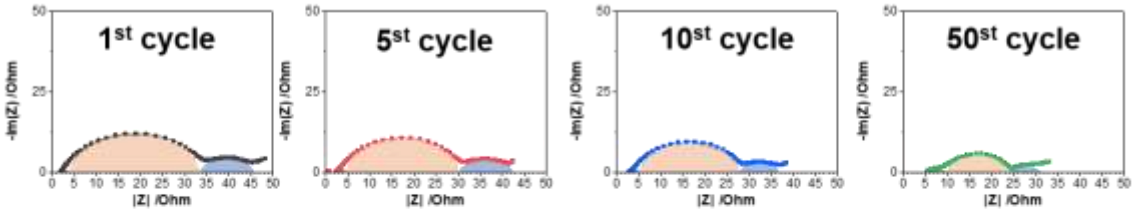

After lithiation (1mAh cm^{-2})	R_b (Ohm)	R_{SEI} (Ohm)	R_{CT} (PETES@Li + Li) (Ohm)
1st Cycle	1.87	2.13	42
5th Cycle	2.29	2.71	37
10th Cycle	2.85	2.35	31.8
50th Cycle	4.8	5.2	21

Fig. S7. Electrochemical impedance spectra fitting results of **a** bare Cu//Li cell and **b** the PETES-Cu//Li cell.

Note: EIS was measured in the state of lithiation with 1mAh cm^{-2} according to the Cu//Li cycle (Fig. 2d and 2e). So, R_{ct} was divided into two parts: Cu electrode and lithium metal electrode, which is the working electrode. In the case of bare-Cu, the R_{SEI} and R_{ct} decrease until the 10th cycle, but due to the unstable interface, the coulombic efficiency drops below 50% at the 50th cycle, and the resistance increases significantly to 140 Ohm again (Fig. S7a). However, in the case of PETES, R_{ct} decreases as the cycle progresses due to stable lithium growth (Fig. S7b).

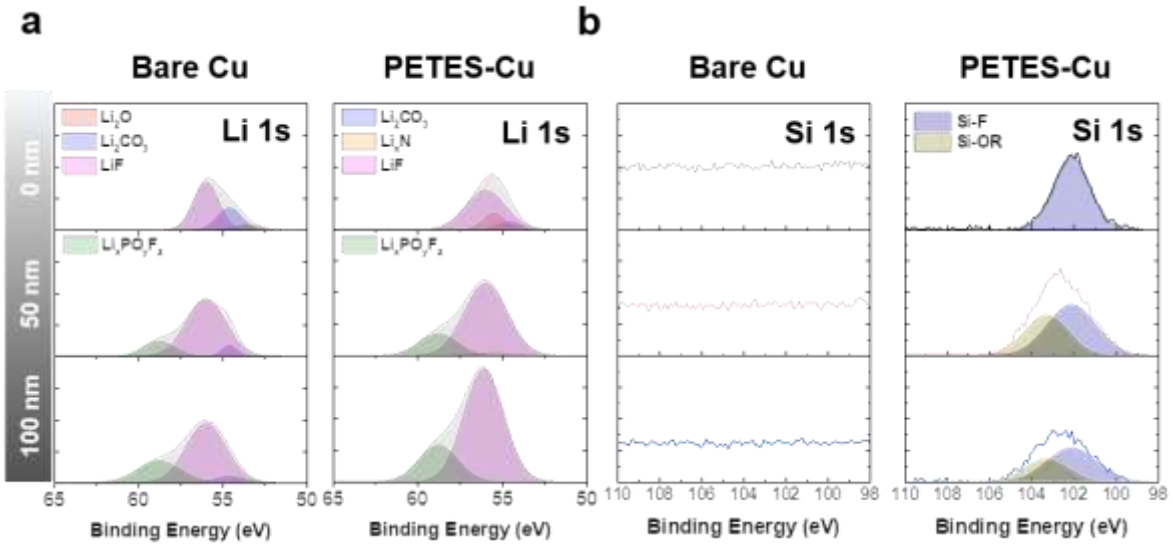

Fig. S8. High-resolution XPS depth profiling for understanding the generation of Si-F bond after pre-cycle at a fixed capacity of 4 mAh cm^{-2} with a current density of 0.5 mA cm^{-2}. **a** Li 1s XPS spectra of bare Cu and PETES-Cu surface and **b** Si 1s XPS spectra of bare Cu and PETES-Cu surface. An average etching depth of samples was ~3 nm for 30s.

Note: Because Figure 4b is taken after plating lithium up to 8 mAh cm^{-2} and characterized Li metal, it was difficult to see Si-F bond formation in PETES. So, after the first lithiation/delithiation, component changes in bare Cu and PETES films were analyzed by XPS, respectively. After the first delithiation, it was confirmed through AFM (Fig. S6) that a stable seed exists in the case of PETES-Cu, and at this time, an abundant LiF layer and Li_xN interface are formed compared to bare-Cu, which can contribute to improving conductivity. As a result of the reaction between PETES and HF in the electrolyte, Si-F bonds dominantly present on the PETES film after delithiation, and as the depth increased, it was confirmed that the SiOR bond of PETES increased.

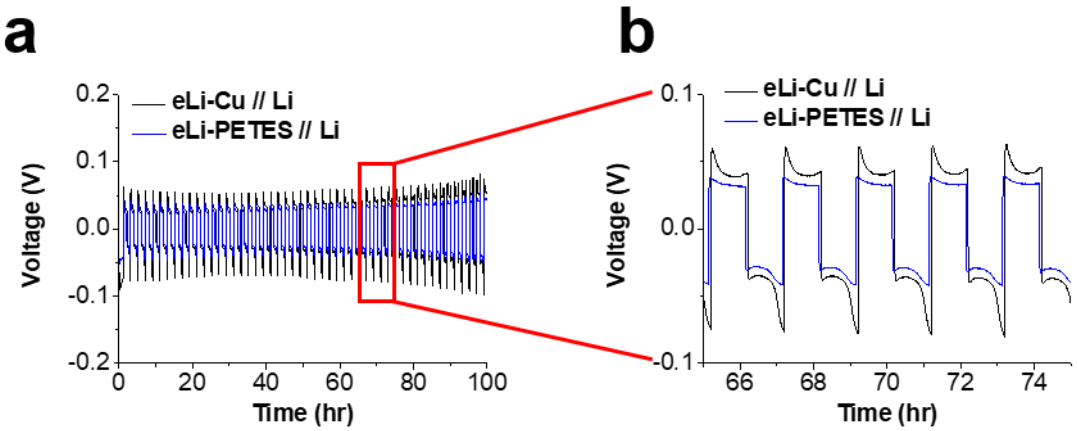

Fig. S9. The electrochemical asymmetric cell test of eLi-Cu//Li (black) and eLi-PETES//Li (blue) with a fixed capacity of 1 mAh cm^{-2} at a current density of 1 mA cm^{-2}. **a** The long-term cycle performance of the asymmetric cell test and **b** the corresponding enlarged image of the selected area.

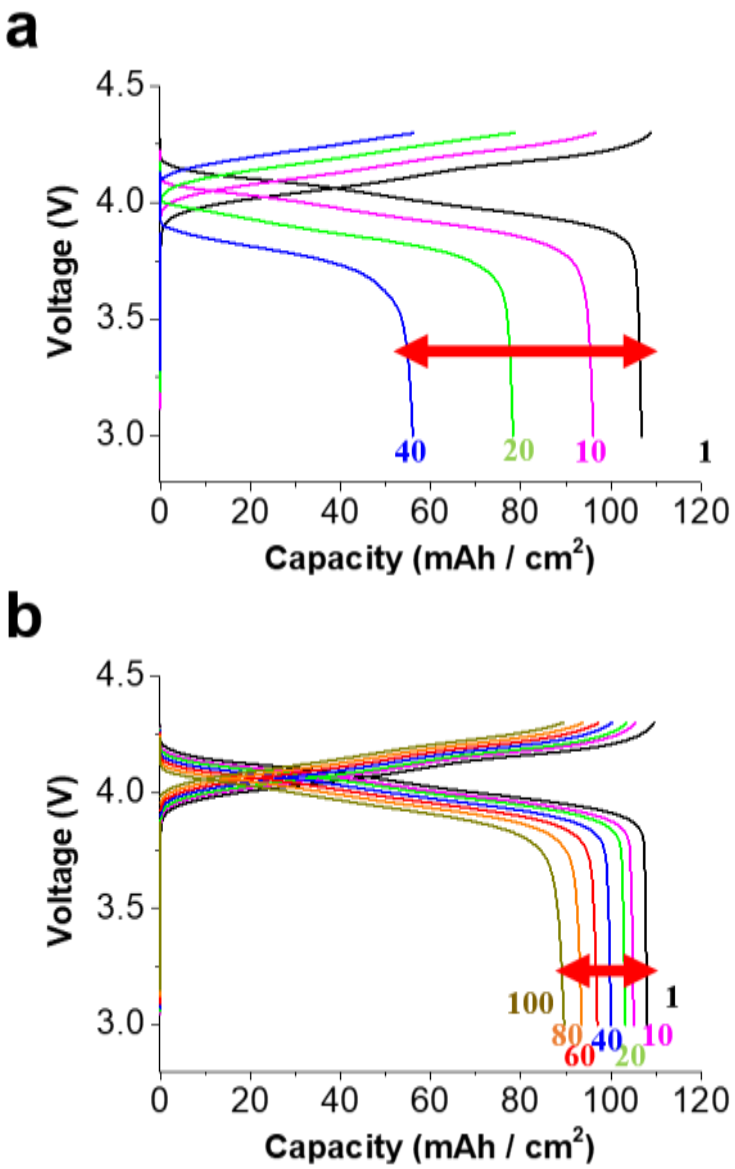

Fig. S10. Voltage profiles of LMO full cells for **a** eLi-Cu and **b** eLi-PETES electrodes.

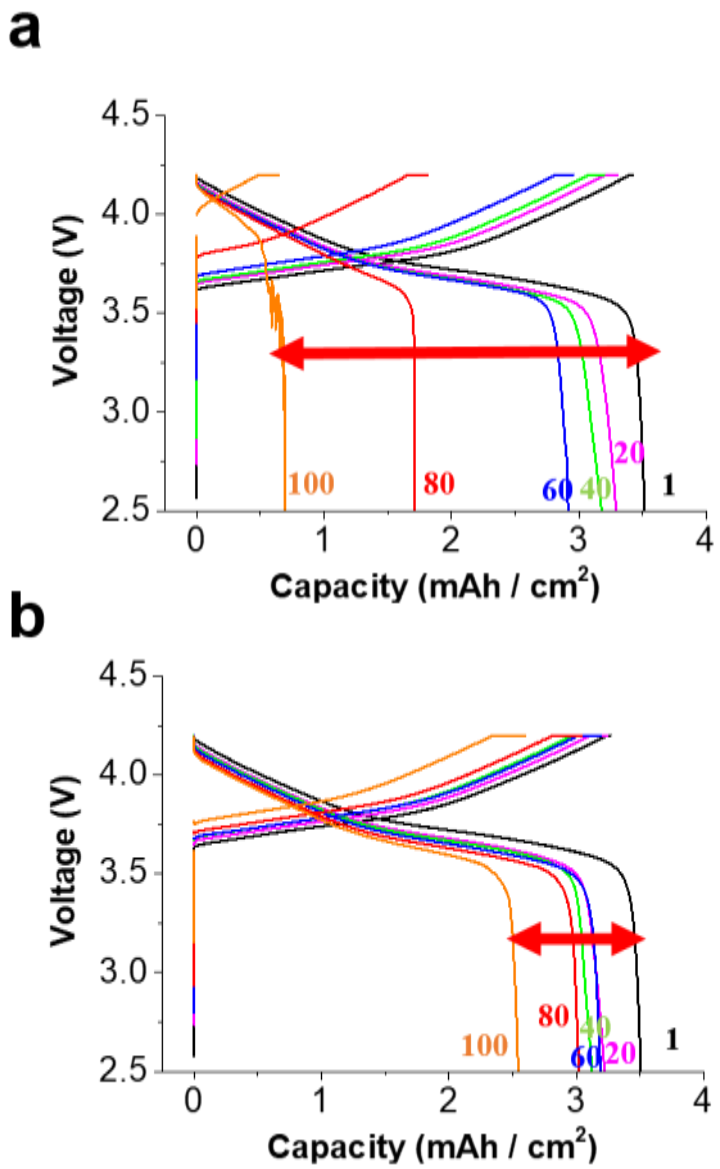

Fig. S11. Voltage profiles of NCM811 full cells for **a** eLi-Cu and **b** eLi-PETES electrodes.

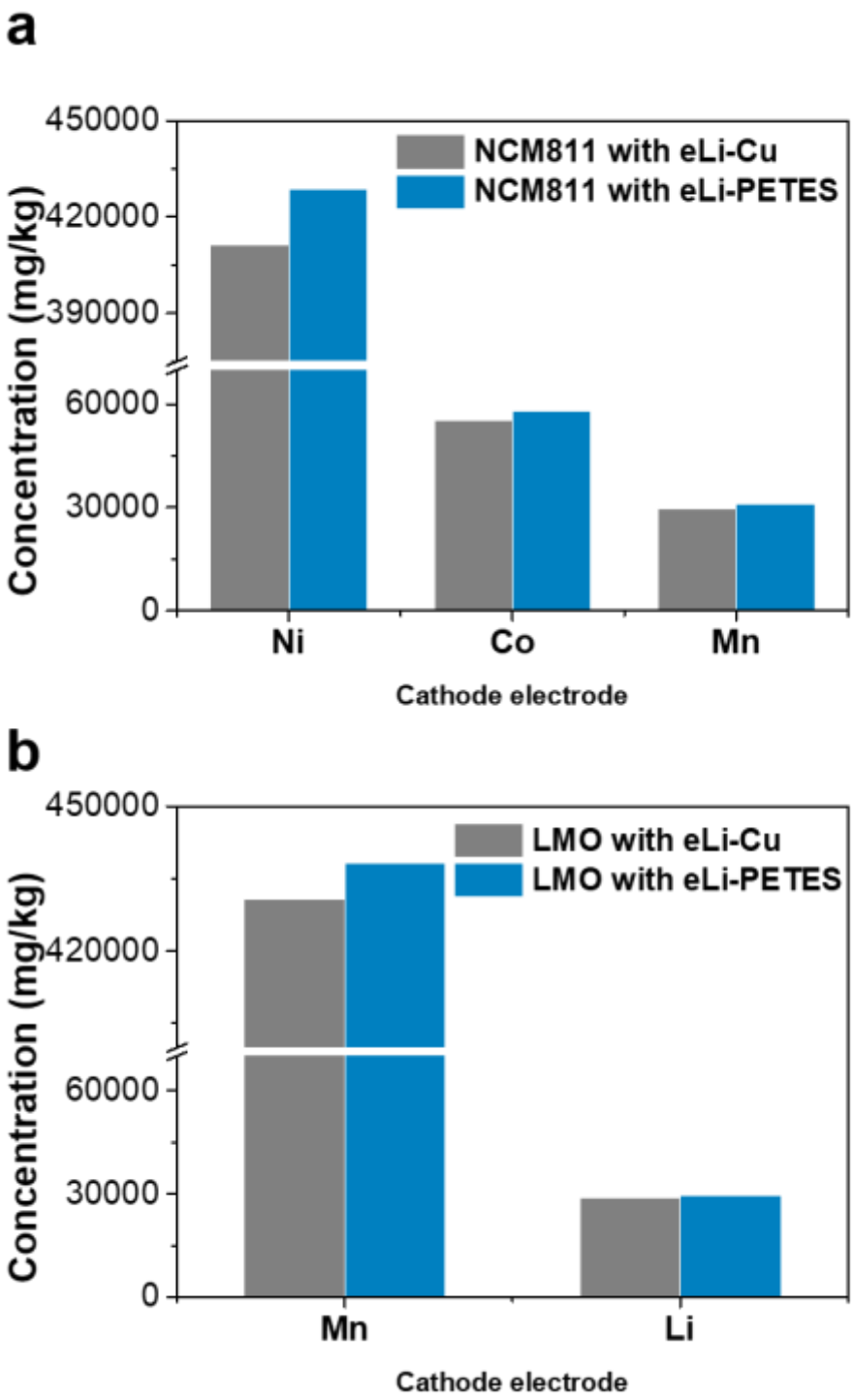

Fig. S12. An inductively coupled plasma optical emission spectrometry (ICP-OES) of the two different cathodes after 50 cycles for **a** NCM811 and **b** LMO. The unstable cycle performance of the eLi-Cu electrode caused a larger Ni and Mn dissolution amount in the cathode than the eLi-PETES electrode.

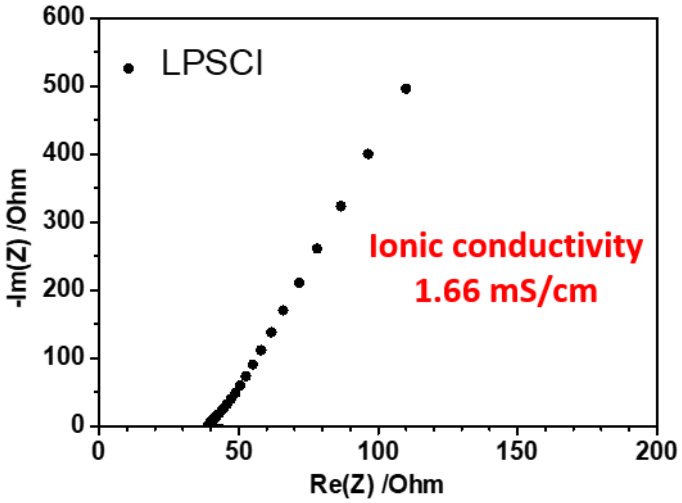

Fig. S13. Nyquist plot for the LPSCl electrolytes and ionic conductivity of composite electrolyte at 25 ℃.

Note. The ionic conductivity of Li_6PS_5Cl is 1.66 mS/cm, which is similar to that reported in other literature.[1,2] Therefore, the reason for the high overpotential of the symmetric cell is not due to the ionic conductivity of the solid electrolyte but the unstable solid-solid interface. Unlike Li-ion batteries, the Li_6PS_5Cl /Li interface has unstable solid-state ionics and interfacial chemistry.[3] Among them, the biggest problem is the high overpotential generated during electron and ion conduction due to interfacial pores. Conventionally, interfacial contact has been improved by using the WIP process for pouch cells[4] or by applying high stack pressure using a stack cells.[5,6] However, the WIP process is inaccessible at laboratory scale and high stack pressures damage the electrodes. In this regard, although the overpotential is relatively high, the coin-type ASSAC is more advantageous for confirming the characteristics of the electrode.

Supplementary Note 1. Discussion of Coulombic efficiency and corresponding cycle performance.

During the beginning of Li deposition on PETES-Cu or bare Cu foil in early cycles, an initial energy barrier needs to be overcome by first forming nucleation sites on the clean working electrode surface, which causes the higher overpotential.[7] Next, in the Li stripping process, the overpotential is induced from the resistance due to the newly formed SEI layer and fresh Li growth on the Li surface.[8] At the end of cycle, the active Li is completely stripped form the working electrode with the cell voltage rising, leaving some dead Li. As a result, the PETES-Cu//Li and bare Cu//Li cells formed an unstable Coulombic efficiency at the early cycles due to the formation of nucleation sites and the SEI layer.

When we use conventional carbonate electrolytes, 1.3M $LiPF_6$-EC/DEC (3/7, v/v) with 10wt% FEC, the Cu//Li cells showed low Coulombic efficiencies of 80~90%.[9,10] This is because dead Li is produced at every cycle, causing continuous volume expansion and SEI formation, eventually depleting the electrolyte.[11,12] However, the PETES film formed the LiF-rich SEI layer and Li seed in first cycle and it causes uniform Li deposition on PETES-Cu electrode. Although conventional carbonate electrolytes are difficult in achieving high Coulombic efficiencies in Cu//Li cells (average CE 80.1% up to 30 cycles), PETES-Cu//Li cells maintained relatively high average Coulombic efficiency of 90.1% up to 30 cycles (Fig. 2c).

Supplementary Note 2. Discussion about full cell performance.

To highlight the advantages of eLi-PETES even in full cells, the test was conducted by setting conditions that could damage the electrolyte as quickly as possible. This is why full cell data is not attractive, and more detailed explanations are as follows: (1) we used conventional carbonate electrolytes, which are rich in F sources but do not allow stable Li electrodeposition in Li metal batteries. (2) In order to clearly confirm the effect of PETES film, we used the electrodeposition method to fabricate Li metal anode. However, the laboratory-scale electrodeposition method cannot follow the characteristics of fabricated Li metal because it does not apply pressure during electrodeposition and does not use an appropriate electrodeposition solution. (3) In addition, we conducted an electrochemical test at high temperature (55℃). $LiPF_6$ based carbonate electrolytes generate parasitic products at high temperatures and exacerbate electrochemical and thermodynamic decomposition.[13-15] However, even under these harsh condition, eLi-PETES showed relatively effective cycle stability, and the results of this study were applied to all-solid-state batteries.

Supplementary References

1. S. Wang, X. Zhang, S. J. Liu, C. Z. Xin, C. J. Xue, F. Richter, L. L. Li, L. Z. Fan, Y. H. Lin, Y. Shen, J. E. G. Janek and C. W. Nan, *J Materiomics*, 2020, **6**, 70-76.
2. C. Yu, S. Ganapathy, J. Hageman, L. van Eijck, E. R. H. van Eck, L. Zhang, T. Schwietert, S. Basak, E. M. Kelder and M. Wagemaker, *Acs Appl Mater Inter*, 2018, **10**, 33296-33306.
3. J. Liu, H. Yuan, H. Liu, C. Z. Zhao, Y. Lu, X. B. Cheng, J. Q. Huang and Q. Zhang, *Advanced Energy Materials*, 2021, **12**.
4. C. H. Wang, J. W. Liang, Y. Zhao, M. T. Zheng, X. N. Li and X. L. Sun, *Energy & Environmental Science*, 2021, **14**, 2577-2619.
5. C. Lee, S. Y. Han, J. A. Lewis, P. P. Shetty, D. Yeh, Y. Liu, E. Klein, H. W. Lee and M. T. McDowell, *Acs Energy Lett*, 2021, **6**, 3261-3269.
6. J. M. Doux, Y. Y. C. Yang, D. H. S. Tan, H. Nguyen, E. A. Wu, X. F. Wang, A. Banerjee and Y. S. Meng, *Journal of Materials Chemistry A*, 2020, **8**, 5049-5055.
7. C. J. Huang, B. Thirumalraj, H. C. Tao, K. N. Shitaw, H. Sutiono, T. T. Hagos, T. T. Beyene, L. M. Kuo, C. C. Wang, S. H. Wu, W. N. Su and B. J. Hwang, Nat Commun, 2021, 12, 1452.
8. J. H. Hyun, M. J. Yi, H. Jung, S. H. Lee, J. H. Um and S. H. Yu, Energy Storage Materials, 2023, 54, 146-155.
9. C. T. Zhou, A. J. Samson, M. A. Garakani and V. Thangadurai, *Journal of the Electrochemical Society*, 2021, **168**.
10. Y. Liu, D. Lin, Y. Li, G. Chen, A. Pei, O. Nix, Y. Li and Y. Cui, *Nat Commun*, 2018, **9**, 3656.
11. K. Yan, Z. Lu, H.-W. Lee, F. Xiong, P.-C. Hsu, Y. Li, J. Zhao, S. Chu and Y. Cui, *Nature Energy*, 2016, **1**.
12. Y. Xiang, M. Tao, X. Chen, P. Shan, D. Zhao, J. Wu, M. Lin, X. Liu, H. He, W. Zhao, Y. Hu, J. Chen, Y. Wang and Y. Yang, *Nat Commun*, 2023, **14**, 177.
13. P. Xiao, R. Luo, Z. Piao, C. Li, J. Wang, K. Yu, G. Zhou and H.-M. Cheng, *Acs Energy Lett*, 2021, **6**, 3170-3179.
14. Z. Geng, J. Lu, Q. Li, J. Qiu, Y. Wang, J. Peng, J. Huang, W. Li, X. Yu and H. Li, *Energy Storage Materials*, 2019, **23**, 646-652.
15. Y. Qiao, Y. He, K. Jiang, Y. Liu, X. Li, M. Jia, S. Guo and H. Zhou, *Advanced Energy Materials*, 2018, **8**.